water

MDPI

Article

Efficiency of Orange Yellow II Degradation by Synergistic Hydroxylamine with Fe^{2+} to Activate Peroxymonosulfate Oxidation: Machine Learning Prediction and Performance Optimization

Runjuan Zhou [1], Kuo Zhang [1] and Ming Zhang [2,*]

[1] School of Chemical and Environmental Engineering, Anhui Polytechnic University, Wuhu 241000, China; rjzhou@126.com (R.Z.); anhzhangk@163.com (K.Z.)
[2] School of Civil Engineering, Anhui Polytechnic University, Wuhu 241000, China
* Correspondence: zhangming@ahpu.edu.cn; Tel.: +86-139-5531-6938

Abstract: A back-propagation neural network (BPNN) was used to model and optimize the process of hydroxylamine (HA)-enhanced Fe^{2+} activating peroxymonosulfate (PMS). Using HA-enhanced Fe^{2+} to activate PMS is a cost-effective method to degrade orange II (AO7). We investigated the individual and interactive effects of the concentrations of Fe^{2+}, HA, and PMS on the degradation of AO7. The R^2 of the BPNN model was 0.99852, and the data were distributed around $y = x$. Sensitivity analysis showed that the relative importance of each factor was as follows: HA > Fe^{2+} > PMS. The optimized results obtained by the genetic algorithm were as follows: the concentration of Fe^{2+} was 35.33 μmol·L^{-1}, HA was 0.46 mmol·L^{-1}, and PMS was 0.93 mmol·L^{-1}. Experiments verified that the AO7 degradation effect within 5 min was 95.7%, whereas the predicted value by the BPNN was 96.2%. The difference between predicted and experimental values is 0.5%. This study provides a new tool (machine learning) to accurately predict the concentrations of HA, Fe^{2+}, and PMS to degrade AO7 under various conditions.

Keywords: advanced oxidation process; machine learning; BPNN; sensitivity analysis; genetic algorithm

check for updates

Citation: Zhou, R.; Zhang, K.; Zhang, M. Efficiency of Orange Yellow II Degradation by Synergistic Hydroxylamine with Fe^{2+} to Activate Peroxymonosulfate Oxidation: Machine Learning Prediction and Performance Optimization. *Water* **2023**, *15*, 1931. https://doi.org/10.3390/w15101931

Academic Editor: Alejandro Gonzalez-Martinez

Received: 22 April 2023
Revised: 8 May 2023
Accepted: 18 May 2023
Published: 19 May 2023

1. Introduction

Azo dye orange yellow II (AO7), as a representative of dye wastewater, which is discharged in large amounts into the environment, can cause adverse reactions, such as skin allergy, dyspnea, and cancer, which seriously threaten human health [1–3]. Based on traditional wastewater treatment technology [4], various methods have been developed to degrade and mineralize AO7 in order to remove it from water. Among them, advanced oxidation technology based on activated persulfate (PS) has been widely used [5,6]. Under heat [7,8], alkali [9], UV [10], transition metal [11], electrochemical, and sonochemical [12,13] action, among others, PS can generate sulfate radicals ($SO_4^{\cdot -}$). The oxidation capacity of sulfate radicals (E_0 = 2.5–3.1 V) is obviously higher than that of PS ($S_2O_8^{2}$: E_0 = 2.1 V; HSO_5: E_0 = 1.82 V) [14]. Compared with other activators, iron salts are widely used as transition metal activators because of their abundance and low price, among which Fe^{2+} salts are more common. However, in the process of Fe^{2+} activating PS, the generation of sulfate radicals is affected by the slow regeneration of Fe^{2+} and the large amount of iron mud generated in the reaction [15,16]. In recent years, studies on the technology of synergistic HA enhancement of Fe^{2+} to activate PS have shown that HA can accelerate the production of Fe^{2+}, slow down the accumulation of iron mud [17–19], and improve the degradation efficiency of pollutants in the system in a wider pH range [20,21].

The process of the Fe^{2+} activation of persulfate is very complex, and various influencing factors and their interactions will change the degradation efficiency. At present,

research on Fe^{2+}-activated persulfate is mainly focused on Fe^{3+} reduction and recycling, the reaction mechanism, and the efficiency of degrading pollutants. There are few studies on Fe^{2+} activating persulfate by the machine learning method. An artificial neural network (ANN) is a machine learning model constructed according to the basic principles of biological neural networks that establishes a nonlinear mapping relationship of input and output neurons through training samples [22]. ANNs have been widely applied in the pollutant removal field for processes such as adsorption, catalytic degradation, and so on [23–25]. An artificial neural model can directly predict the final state of the pollutant treatment system and guide the process of wastewater treatment. By reducing the number of experiments, processing costs can also be reduced by the use of ANN [26]. In addition, the influence degree of input factors and their interactions on degradation efficiency can be determined through the neural network model. Because of the complexity of advanced oxidation technology, it is important to develop a model to analyze the process of synergistic Fe^{2+} to activate PMS. Establishing a neural network model of the process can provide valuable guidance in order to improve the degradation effect and further understand the degree of influence of each factor and their interactions on the pollutant degradation effect.

However, the physical interpretation of the intermediate process of neural networks has always been an unsolved "black box" problem. The Garson and PaD2 algorithms can solve this problem to a certain extent and reveal the degree of influence of each factor on the model response value. Therefore, in this study, the Garson and PaD2 algorithms combined with ANN were applied to investigate the degradation of AO7 in the HA/Fe^{2+}/PMS system so that the key factors affecting degradation efficiency and the effect of the interaction of various factors on degradation could be determined.

Based on the above research, in this study, ANN was used to fit the process of synergistic HA and Fe^{2+} to activate PMS for the degradation of AO7. The Garson and PaD2 algorithms were used to analyze the sensitivity of the neural network. A coupled intelligent algorithm of the neural network and genetic algorithm was constructed, with the genetic algorithm embedded into the neural network to optimize the extreme value, and the optimal process conditions of the synergy of HA with Fe^{2+} to activate PMS for the degradation of AO7 were obtained. The main contributions of this study are as follows: First, we propose an approach to describe the relationship between influencing factors and degradation efficiency by means of modeling. Second, we optimized the combination of reaction conditions with the best degradation rate on the basis of modeling, which can reduce the amount of trial and error. Third, we introduce the Garson and PaD2 algorithms in machine learning theory, which can be used for sensitivity analysis of influencing factors to obtain their importance ranking.

2. Materials and Methods

2.1. Reagents and Instruments

AO7 ($C_{16}H_{11}N_2NaO_4S$), hydroxylamine sulfate ($H_6N_2O_2 \cdot H_2SO_4$), $FeSO_4 \cdot 7H_2O$, potassium bisulfate ($KHSO_5 \cdot 0.5KHSO_4 \cdot 0.5K_2SO_4$), ethanol ($C_2H_5OH$), and reagents were analytically pure, purchased from Aladdin Pharmaceuticals, Shanghai, China. All water used in the experiment was ultra-pure water.

An ultraviolet–visible spectrophotometer (UV-3600, Shimadzu, Kyoto, Japan), temperature-controlled magnetic stirrer with digital display (85-2 type, Jintan Dadi Automation Instrument, Changzhou, China), and FA2004 electronic scale (FA2004, Sunny Hengping Instrument, Shanghai, China) were used.

2.2. Experimental Methods

All experiments were carried out in 250 mL beakers with constant stirring at 20 ± 1 °C. Solutions of AO7, Fe^{2+}, and HA were evenly mixed, and then the specified amount of PMS was added to start the reaction. The initial volume of the mixture was kept at 50 mL. At the fifth minute of reaction, 1 mL of reaction solution was extracted and quenched with 1 mL of ethanol. The concentration of the solution was measured using a UV spectrophotometer.

The experiments were carried out against the background pH of the mixed solution. All experiments were repeated in triplicate. The methods of determining the concentrations of AO7 and Fe^{2+} are described in previous studies [20,21]. Based on the results of the single-factor experiment, the concentration range of each influencing factor was determined. The initial concentration of AO7 was 100 mg/L, and the initial pH of the solution was 4.7. The reaction time of all experiments was set at 5 min.

2.3. BP Neural Network Model

MATLAB R2016b software (MathWorks Inc., Natick, MA, USA) was used to establish the BP neural network model. The BP neural network (BPNN) is a kind of multilayer feed-forward neural network, and is one of the most widely used ANN models. It consists of one input layer, one hidden layer, and one output layer [27]. In this study, a typical 3-layer BPNN was used [28]. The concentrations of HA, Fe^{2+}, and PMS were the input variables, and the degradation efficiency of AO7 was the output variable. Based on the single-factor experiment, the experimental variables and coding levels were obtained, as shown in Table 1 [20,21], and the Box–Behnken design (BBD) method was adopted to design the experiment, as shown in Table 2. In order to avoid the impact of data dimension, the data were processed without dimension. The Premnmx function in MATLAB was used to normalize the data. The experimental data were randomly allocated according to the following proportions: training set 70%, verification set 15%, and test set 15%. The influence of different hidden layer node numbers, training function, and excitation function on the BPNN was investigated by trial and error to determine the optimal structure of the BPNN. The root mean square error (RMSE) was used as the performance evaluation index for the neural network; the lower the RMSE value, the better the performance of the neural network.

Table 1. Experimental variables and coding levels.

Factors	Levels		
	−1	**0**	**+1**
Concentration of Fe^{2+} ($\mu mol \cdot L^{-1}$)	10	25	40
Concentration of HA ($mmol \cdot L^{-1}$)	0.1	0.3	0.5
Concentration of PMS ($mmol \cdot L^{-1}$)	0.5	0.75	1

Table 2. Experimental scheme and predicted BPNN values.

Runs	Fe^{2+} ($\mu mol \cdot L^{-1}$)	HA ($mmol \cdot L^{-1}$)	PMS ($mmol \cdot L^{-1}$)	R_{AO7} (%)	
				Actual	**Predicted**
1	40	0.1	0.75	66.9	66.9
2	10	0.5	0.75	73.8	73.8
3	25	0.3	0.75	86.1	86.1
4	25	0.3	0.75	86.1	86.1
5	10	0.3	1	58.7	58.7
6	40	0.5	0.75	94.9	94.9
7	25	0.3	0.75	85.7	86.1
8	10	0.3	0.5	69.5	69.5
9	25	0.5	1	91.8	91.8
10	25	0.5	0.5	83.5	83.5
11	40	0.3	1	92.8	92.8
12	25	0.1	0.5	63.7	63.7
13	25	0.3	0.75	86.4	86.1
14	10	0.1	0.75	43.1	44.9
15	25	0.3	0.75	85.7	86.1
16	40	0.3	0.5	80.5	80.5
17	25	0.1	1	55.1	56.4

2.4. Garson and PaD2 Algorithms

Sensitivity analysis assumes that the model is of the form $y = f(x_1, x_2, \cdots, x_n)$ (where x_i is the ith factor value of the model), and it determines the degree of influence of each factor on the response value of the model when the range changes. The sensitivity coefficient represents the factor's influence degree. The larger the sensitivity coefficient, the greater the influence of the factor on the response value of the model. Based on different analysis objects, sensitivity analysis can be divided into local and global sensitivity analysis. Local sensitivity analysis examines the influence of a single factor on the response value of the model, while global sensitivity analysis examines the impact of multiple factors on the response value of the model at the same time, as well as the impact of the interaction between factors [29]. The Garson algorithm is a local sensitivity analysis method based on the connection weights of a neural network. Through the connection weights, the degree of influence of a single factor on the response value of the model is calculated [30]. The PaD2 algorithm is used to analyze the influence of the interaction of two factors on the response value of the model. It is assumed that the topological relationship of the BPNN is M-N-1, and the network output form is $y = f(x_1, x_2, \cdots, x_n)$. By solving the second partial derivative of the equation, the degree of influence of the interaction between the two factors on the response value of the model can be analyzed [31]. In this study, the Garson algorithm (Equation (1)) was used to analyze local sensitivity, and the PaD2 algorithm (Equation (2)) was used to analyze global sensitivity.

$$Garson_{ik} = \frac{\sum_{j=1}^{N} \frac{|w_{ij}||v_{jk}|}{\sum_{r=1}^{M}|w_{rj}|}}{\sum_{i=1}^{M}\sum_{j=1}^{N} \frac{|w_{ij}||v_{jk}|}{\sum_{r=1}^{M}|w_{rj}|}} \tag{1}$$

Here, $Garson_{ik}$ is the sensitivity coefficient of the ith input variable to the kth output variable, M is the number of neurons in the input layer, N is the number of hidden layer neurons, L is the number of neurons in the output layer, w_{ij} is the weight of the connection between the ith neuron in the input layer and the jth neuron in the hidden layer, and v_{jk} is the weight of the connection between the jth neuron of the hidden layer and the kth neuron of the output layer.

$$d_{ik}^{t} = f'\left(net^{t}\right)\left[f'\left(net^{t}\right)\sum_{j=1}^{N} w_{ij}v_{j}f'\left(net_{j}^{t}\right)\sum_{j=1}^{N} w_{kj}v_{j}f'\left(net_{j}^{t}\right) + \sum_{j=1}^{N} w_{ij}w_{kj}v_{j}f''\left(net_{j}^{t}\right)\right] \tag{2}$$

Here, ${d_{ik}}^{t}$ is the sensitivity coefficient of factors x_i and x_k of the tth sample to response value y, N is the number of hidden layer neurons, w_{ij} is the weight of the connection between the ith neuron in the input layer and the jth neuron in the hidden layer, w_{kj} is the weight of the connection between the kth neuron in the input layer and the jth neuron in the hidden layer, v_j is the weight of the connection between the jth neuron in the hidden layer and the neuron in the output layer, $f'(net^t)$ is the first partial derivative of the excitation function of the neurons in the output layer, $f'(net_j{}^t)$ is the first partial derivative of the excitation function of the hidden layer neuron, and $f''(net_j{}^t)$ is the second partial derivative of the excitation function of the hidden layer neuron.

The overall sensitivity coefficient of x_i and x_k to response value y is shown in Equation (3):

$$Sd_{ik} = \sum_{i=1}^{m}\left(d_{ik}^{t}\right)^{2} \tag{3}$$

where Sd_{ik} is the overall sensitivity coefficient of x_i and x_k to the response value y and m is the total number of samples.

3. Results and Discussion

3.1. Determination of the BPNN Structure

The number of hidden layer neurons affects the accuracy of the BPNN by affecting the convergence performance of the error function. The number of hidden layer neurons is estimated to be in the range of 3–12 according to empirical Equation (4) [32]. The number of hidden layer neurons was determined by trial and error, and the result is shown in Figure 1a.

$$N = \sqrt{A + B} + C \tag{4}$$

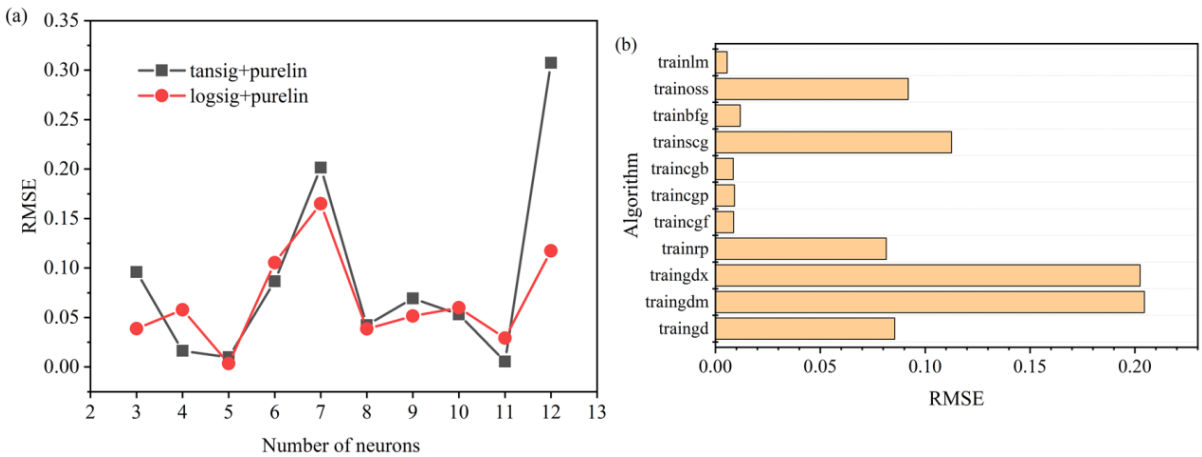

Figure 1. (**a**) Influence of number of hidden layer neurons and excitation function; (**b**) training function on performance of BPNN.

Here, N is the number of hidden layer neurons, A is the number of neurons in the input layer, B is the number of neurons in the output layer, and C is a positive integer between 1 and 10.

The excitation function of the hidden layer in the BPNN generally selects an S-type function, which is divided into a logarithmic function (logsig) and a hyperbolic tangent function (tansig), and the excitation function of the output layer is generally selected as a linear function (purelin). In this study, we investigated the effects of the combination of two excitation functions (logsig + purelin and tansig + purelin) on the performance of the BPNN. The result is displayed in Figure 1a. We compared the effects of 11 training functions, including the gradient descent algorithm (traingd), elastic BP algorithm (trainrp), and the Levenberg–Marquardt algorithm (trainlm), on the performance of the BPNN. The results are shown in Figure 1b.

Through analysis and comparison, the topology structure of the BPNN finally adopted in this study was 3-11-1. The excitation functions used in the hidden and output layers were tansig and purelin functions, respectively, and the training function was trainlm. The optimal BPNN structure is shown in Figure 2.

3.2. Performance Evaluation of the BPNN

Figure 3 shows the performance curve of the BPNN. The smaller the MSE value, the higher the accuracy of the BPNN in data prediction. As can be seen in Figure 3, the error of the verification set decreased with the decrease in error of the training set, but did not increase. At the fifth iteration of the BPNN, the error of verification set reached the minimum value of 0.0025177, indicating that there was no overfitting in the BPNN training process. After three iterations, the error of the test set remained stable and was lower than that of the verification set, indicating that the established BPNN model had good generalization ability.

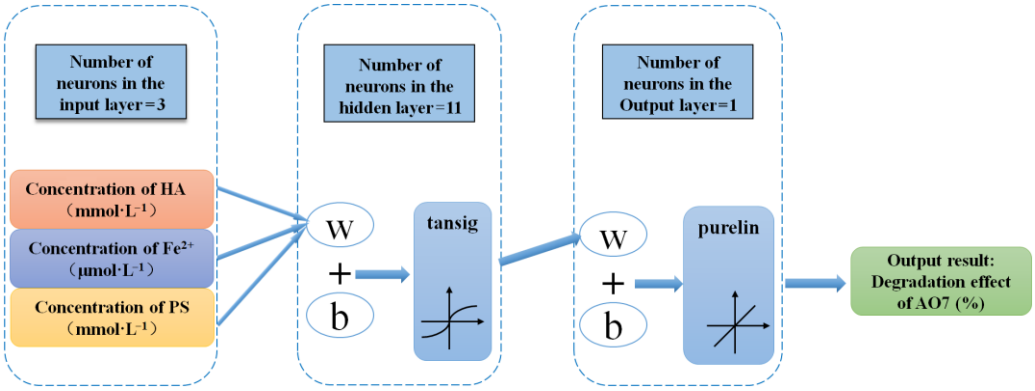

Figure 2. Structure diagram of BPNN.

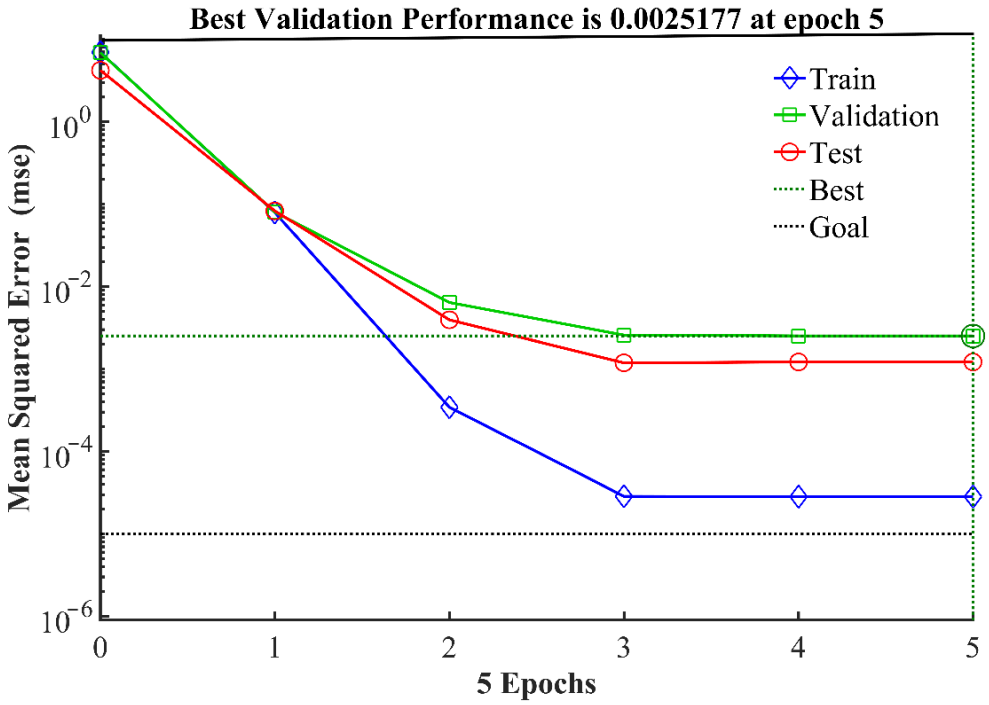

Figure 3. Performance curve of BPNN.

Figure 4 shows the linear fitting diagram of the BPNN. The larger the value of R^2, the better the BPNN fits. The R^2 of the training set is 0.99985, indicating that the model can explain 99.985% of the response value changes. The R^2 of the verification set is 0.99628, that of the test set is 0.99660, and that of all sets is 0.99852. The data are distributed near the line $y = x$, indicating that the error between measured and predicted value is small. The BP neural network has good predictive ability and a nonlinear mapping relationship.

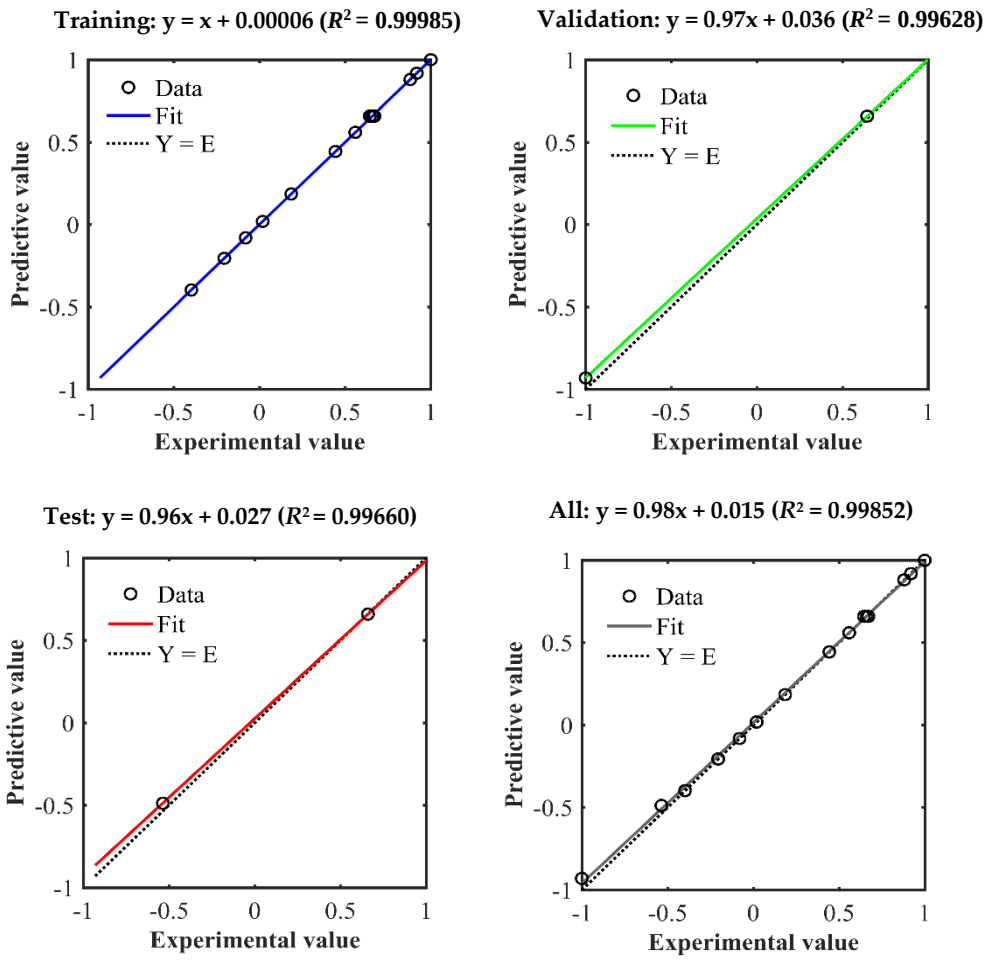

Figure 4. Linear fitting diagrams of BPNN.

The final result of the trained BPNN's predicted values is given in Table 2, and the model training result is shown in Figure 5.

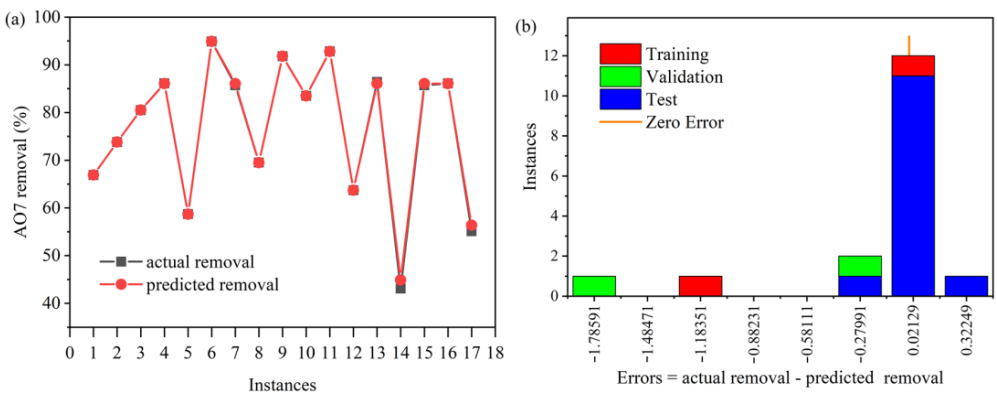

Figure 5. BPNN model training results: (**a**) comparison of predicted and measured values; (**b**) histogram of residuals.

It can be seen from Figure 5a that the error between the predicted and measured values was very small. In addition, it can be seen in Figure 5b that the error was mainly concentrated near the zero point. The above results show that the predicted values of the model based on the BPNN are in good agreement with the measured values, verifying the

reliability and accuracy of the selected BPNN model. The results indicate a good fit of the BPNN model for the process of synergistic hydroxylamine with Fe^{2+} to activate PMS.

3.3. Sensitivity Analysis of the BPNN

The weight and threshold values are listed in Table 3.

Table 3. Weights and thresholds of BPNN.

Hidden Layer Neuron	Weight between Input and Hidden Layers			Threshold of Hidden Layer	Weight between Hidden and Output Layers	Threshold of Output Layer
	Fe^{2+}	HA	PMS			
1	2.8783	−0.7327	−1.1964	−3.0276	−0.1574	
2	−2.1334	−2.3543	−0.2061	2.3871	−0.0495	
3	−1.8180	2.3485	−0.3131	2.0163	−0.1829	
4	−0.1180	2.9386	−0.7082	1.4494	0.5138	
5	−2.9141	−0.9853	0.4082	0.6374	−0.0003	
6	1.6788	1.6654	2.0006	0.1730	0.2882	−0.2901
7	−1.1376	−2.5627	−1.2200	−0.8487	0.0315	
8	3.0577	0.2525	−0.3583	1.2881	0.2380	
9	−0.7018	2.0271	−2.2731	−1.8713	−0.0537	
10	1.0895	0.7200	−2.6689	2.7863	0.3428	
11	−2.4593	−1.3092	−1.6007	−2.9865	0.0662	

According to the Garson algorithm, based on neural network weights, the order of influence of each factor on the degradation of AO7 is as follows: concentration of HA (39.6%) > Fe^{2+} (32.4%) > PMS (28%). According to the PaD2 algorithm, the order of influence of the interaction of two factors on the degradation effect is as follows: concentration of Fe^{2+} and PMS (7.54) > concentration of HA and PMS (5.97) > concentration of Fe^{2+} and HA (2.21).

3.4. Influence of Concentrations of Fe^{2+}, HA, and PMS on Degradation of AO7

According to the BPNN model, the nonlinear mapping relationship between the concentrations of Fe^{2+}, HA, and PMS and the degradation of AO7 were obtained. Origin 2018 software was used to make a three-dimensional surface map, and the results are shown in Figure 6. Each surface map shows the interaction of only two factors on the response value of the model, with the other factors remaining at the central level.

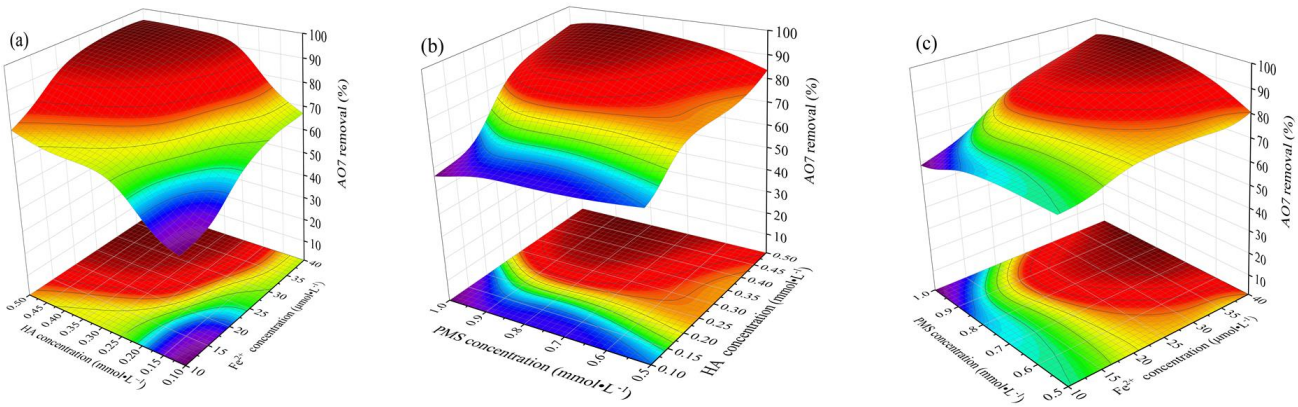

Figure 6. Effects on degradation of AO7. Interaction between concentrations of (**a**) HA and Fe^{2+}, (**b**) HA and PMS, and (**c**) PMS and Fe^{2+}.

According to Figure 6a,b, increasing the concentration of HA can improve the degradation of AO7. A sufficient amount of HA can rapidly reduce the Fe^{3+} to Fe^{2+}, so that there will be a sufficient amount of Fe^{2+} in the system to activate PMS and produce $SO_4^{\bullet-}$ to degrade AO7 [33]. Similarly, it can be seen from Figure 6a,c that the efficiency of degrading

AO7 increased with increased concentration of Fe^{2+}. Increasing the concentration of Fe^{2+} can activate PMS to produce more $SO_4^{\bullet-}$, thus improving the degradation effect.

It can also be seen from Figure 6b that when the concentration of HA is low, increasing the concentration of PMS would reduce the degradation of AO7. In the reaction system, the excessive PMS would compete with the target pollutant and react with $SO_4^{\bullet-}$, reducing the amount of $SO_4^{\bullet-}$ in the system [34,35], and thus reducing the degradation effect. When the concentration of HA is high, increasing the concentration of PMS could improve the degradation of AO7. These results further show that there was an obvious interaction between the concentrations of HA and PMS.

The chemical reaction of PMS and $SO_4^{\bullet-}$ is shown in Equation (5):

$$HSO_5^- + SO_4^{\bullet-} \rightarrow SO_4^{2-} + SO_5^{\bullet-} + H^+ \quad (5)$$

According to Figure 6c, when the concentration of Fe^{2+} is low, increasing the concentration of PMS would reduce the degradation of AO7. When the concentration of Fe^{2+} is high, increasing the concentration of PMS would improve the degradation effect. These results further show that the interaction between the concentration of Fe^{2+} and the concentration of PMS was significant.

3.5. Optimization of Process Parameters

The genetic algorithm is a method of seeking the optimal solution by simulating biological evolution in nature. It is widely used to solve complex global optimization problems and is highly robust [36,37]. Using a neural network to fit an uncertain nonlinear function and embedding it into the genetic algorithm to form a hybrid intelligent algorithm has been successfully applied to combinatorial optimization in the environmental field. The extreme value optimization process of the genetic algorithm embedded with BPNN is shown in Figure 7.

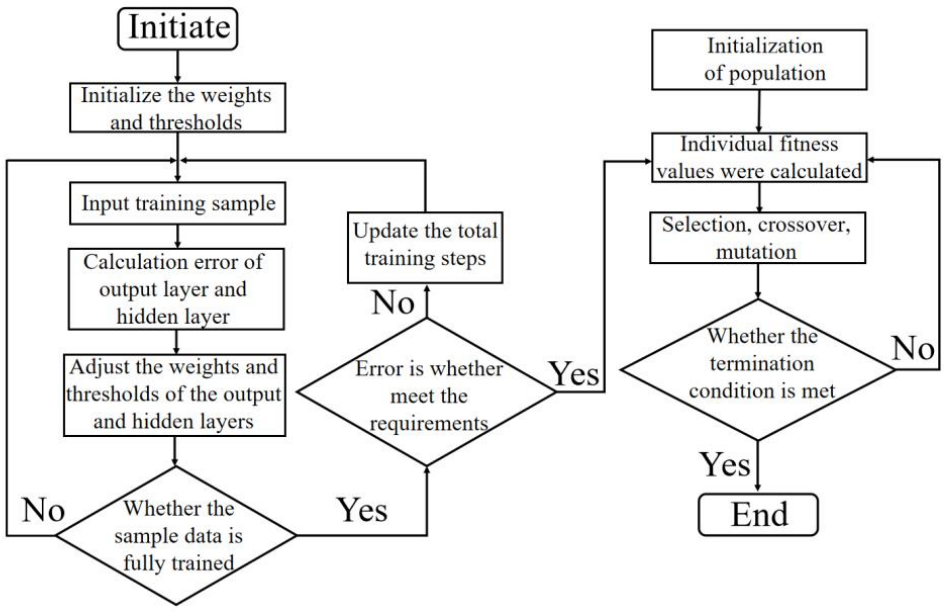

Figure 7. Flowchart of BPNN embedded in genetic algorithm for extreme value optimization.

For the best degradation of AO7, global optimization of the genetic algorithm was carried out, and the optimized conditions are shown in Table 4.

Table 4. Optimized conditions and actual degradation rates.

No.	Optimized Conditions	Predicted Degradation Rate	Actual Degradation Rate	Mean; Error
1	Fe^{2+}: 35.33 μmol·L^{-1},		96.0%	
2	HA: 0.46 mmol·L^{-1},	96.2%	95.4%	95.7%; −0.5%
3	PMS: 0.93 mmol·L^{-1}		95.6%	

The optimized reaction conditions in Table 4 are different from the central point conditions in Table 2, and the removal rate after optimization is larger than the single-factor experimental results, which shows that the modeling and optimization in this study were necessary. The verification experiments showed that the degradation rate of AO7 was 95.7%, which was only 0.5% lower than the model's predicted value of 96.2%. The results show that the optimal combination of concentrations of Fe^{2+}, HA, and PMS can be obtained by combining BPNN with the genetic algorithm. Using this combination, the ideal AO7 degradation rate can be obtained, and the error is small. Therefore, BPNN combined with the genetic algorithm can be used to optimize the parameters of AO7 degradation in the HA/Fe^{2+}/PMS system.

4. Conclusions

In this study, we used a BP neural network model to improve the degradation rate of AO7 using the HA/Fe^{2+}/PS advanced oxidation system. At the beginning of the study, we obtained the level of each reaction condition based on the results of a single-factor experiment, and we designed the experimental scheme according to the Box–Behnken design. Then we obtained the degradation rate of AO7 according to each experimental scheme, trained the BP neural network, and established the neural network model. In order to obtain the sensitivity of each reaction condition to the degradation rate, Garson and PaD2 algorithms were innovatively introduced, showing the novelty of this study. Finally, we carried out three verification experiments based on the optimized reaction conditions. The experimental results show the advantages of modeling and optimization in this study. The conclusions are as follows:

(1) The final BPNN topology was 3-11-1. The excitation functions used in the hidden and output layers were tansig and purelin, respectively, and the training function was trainlm. The R^2 of the established BPNN model was 0.99852, and the data were distributed near the line y = x. The results show that the predicted value based on the BP neural network model was in good agreement with the measured value, and that there was a good fit of the model for the process of synergistic hydroxylamine with Fe^{2+} to activate PMS.

(2) Using the Garson and PaD2 algorithms based on the neural network weights, the order of influence of factors and factor pairs on the degradation of AO7 was calculated as follows: concentration of HA > Fe^{2+} > PMS, and concentrations of Fe^{2+} and PMS > concentrations of HA and PMS > concentrations of Fe^{2+} and HA.

(3) The optimization result obtained by the genetic algorithm was as follows: the concentration of Fe^{2+} was 35.33 μmol·L^{-1}, HA was 0.46 mmol·L^{-1}, and PMS was 0.93 mmol·L^{-1}. According to the verification experiment, the degradation of AO7 was 95.7%, which was only 0.5% lower than the model's predicted value, 96.2%.

The above results show that the BP neural network can indeed improve the degradation rate of AOP systems, and the modeling results are reasonable, and can be used as a reference in the research of other AOP systems. However, this study also has some limitations, which should be considered in future studies. Whether the conclusions of this study are applicable to pollution other than AO7 is unknown, and other types of pollutants need to be explored. Other AOP systems are not reflected in this study, and more systems should be studied. Although the Garson and PaD2 algorithms are introduced in this study to obtain some useful conclusions about parameter sensitivity, the constructed BP neural

network is still a black box lacking interpretability, which is also part of the next step of research to focus on.

Author Contributions: Conceptualization, R.Z. and M.Z.; methodology, K.Z.; validation, K.Z. and R.Z.; writing—original draft preparation, R.Z.; writing—review and editing, K.Z. and M.Z.; visualization, K.Z.; funding acquisition, R.Z. and M.Z. All authors have read and agreed to the published version of the manuscript.

Funding: This research was funded by the Anhui Provincial Natural Science Foundation (2208085QE176, 2008085ME159), the Key Project of the University Natural Science Research Project of Anhui Province (KJ2021A0505), and the Science and Technology Project of Wuhu City (2022jc15).

Data Availability Statement: The raw data supporting the conclusion of this article will be made available by the authors without undue reservation.

Acknowledgments: We want to acknowledge the journal editors and anonymous reviewers for their valuable comments.

Conflicts of Interest: The authors declare no conflict of interest.

References

1. Qu, S.; Wang, W.; Pan, X.; Li, C. Improving the Fenton catalytic performance of FeOCl using an electron mediator. *J. Hazard. Mater.* **2020**, *384*, 121494. [CrossRef] [PubMed]
2. Qin, Q.D.; Qiao, N.; Liu, Y.H.; Wu, X. Spongelike porous CuO as an efficient peroxymonosulfate activator for degradation of Acid Orange 7. *Appl. Surf. Sci.* **2020**, *521*, 1464792020. [CrossRef]
3. Al-Musawi, T.J.; Rajiv, P.; Mengelizadeh, N.; Mohammed, I.A.; Balarak, D. Development of sonophotocatalytic process for degradation of acid orange 7 dye by using titanium dioxide nanoparticles/graphene oxide nanocomposite as a catalyst. *J. Environ. Manag.* **2021**, *292*, 112777. [CrossRef] [PubMed]
4. Sun, Z.H.; Li, S.; Ding, H.J.; Zhu, Y.H.; Wang, X.X.; Liu, H.F.; Zhang, Q.; Zhao, C. Electrochemical/Fe^{3+}/peroxymonosulfate system for the degradation of Acid Orange 7 adsorbed on activated carbon fiber cathode. *Chemosphere* **2020**, *241*, 125125. [CrossRef]
5. Zhu, K.M.; Wang, X.S.; Chen, D.; Ren, W.; Lin, H.; Zhang, H. Wood-based biochar as an excellent activator of peroxydisulfate for Acid Orange 7 decolorization. *Chemosphere* **2019**, *231*, 32–40. [CrossRef] [PubMed]
6. Liu, F.Z.; Yi, P.; Wang, X.; Gao, H.; Zhang, H. Degradation of Acid Orange 7 by an ultrasound/ZnO-GAC/persulfate process. *Sep. Purif. Techno.* **2018**, *194*, 181–187. [CrossRef]
7. Zhu, S.R.; Gao, N.Y.; Lu, X.; Guo, Y.L. Degradation of bisphenol A in aqueous solution by thermally activated sulfate oxidation. *Chin. Environ. Sci.* **2017**, *37*, 188–194.
8. Rahmani, A.; Salari, M.; Tari, K.; Shabanloo, A.; Shabanloo, N.; Bajalan, S. Enhanced degradation of furfural by heat-activated persulfate/nZVI-rGO oxidation system: Degradation pathway and improving the biodegradability of oil refinery wastewater. *J. Environ. Chem. Eng.* **2020**, *8*, 104468. [CrossRef]
9. Li, Z.Y.; Wang, L.; Liu, Y.L.; He, P.N.; Ma, J. Overlooked enhancement of chloride ion on the transformation of reactive species in peroxymonosulfate/Fe(II)/NH_2OH System. *Water Res.* **2021**, *195*, 116973. [CrossRef]
10. Dhaka, S.; Kumar, R.; Khan, M.A.; Paeng, K.J.; Kurade, M.B.; Kim, S.J.; Jeon, B.H. Aqueous phase degradation of methyl paraben using UV-activated persulfate method. *Chem. Eng. J.* **2017**, *321*, 11–19. [CrossRef]
11. Wang, H.B.; Wang, Q.; Liu, Y.Q.; Fu, Y.S.; Wu, P. Degradation of diclofenac by ferrous activated persulfate. *Environ. Chem.* **2020**, *39*, 869–875.
12. Rahmani, A.; Shabanloo, A.; Shabanloo, N. A mini-review of recent progress in lead dioxide electrocatalyst for degradation of toxic organic pollutants. *Mater. Today Chem.* **2023**, *27*, 101311. [CrossRef]
13. Rahmani, A.; Shabanloo, A.; Shabanloo, N.; Torkshavand, Z.; Dargahi, A.; Ansari, A. The integration of PbO_2-based EAOPs with other advanced oxidation processes for improved treatment of water and wastewater. *Curr. Opin. Electrochem.* **2023**, *37*, 101204. [CrossRef]
14. Ghanbari, F.; Moradi, M. Application of peroxymonosulfate and its activation methods for degradation of environmental organic pollutants: Review. *Chem. Eng. J.* **2016**, *310*, 307–315. [CrossRef]
15. Wang, W.; Zhang, H.; Chen, Y.; Shi, H. Efficient Degradation of Tetracycline via Coupling of Photocatalysis and Photo-Fenton Processes over a 2D/2D α-Fe_2O_3/g-C_3N_4 S-Scheme Heterojunction Catalyst. *Acta Phys.-Chim. Sin.* **2022**, *38*, 2201008. [CrossRef]
16. Su, C.; Li, R.; Li, C.; Wang, W. Piezo-promoted regeneration of Fe^{2+} boosts peroxydisulfate activation by $Bi_2Fe_4O_9$ nanosheets. *Appl. Catal. B-Environ.* **2022**, *310*, 121330. [CrossRef]
17. Li, C.W.; Chi, K.Y.; Yang, W.W.; Li, S.; Du, J. Remediation effect of alkali-activate persulfate in groundwater of a chlorinated hydrocarbon contaminated site. *Chin. J. Environ. Eng.* **2021**, *15*, 1916–1926.
18. Li, X.; Feng, S.; Yang, J.; Xie, T.; Wang, J.; Chen, X.; Kong, D.; Chen, H. Tetracycline removal by a magnetic heterojunction $Cu_2O/CoFe_2O_4$ activating peroxymonosulfate. *Rare Metals* **2023**, *42*, 862–874. [CrossRef]

19. Xu, W.X.; Wu, J.F.; Xing, J.M.; Gong, Q.; Nie, H.; Wang, S.L. Degradation of acetaminophen by hydroxylamine enhanced Fe^{2+}/persulfate system. *Acta Sci. Circumstantiae* **2019**, *39*, 3410–3417.
20. Zhang, K.; Zhang, M.; Zhou, R.J.; Zhou, T. Hydroxylamine-enhanced Fe(II)-peroxymonosulfate activation for efficient degradation of organic pollutants: Optimization by response surface methodology. *Water Sci. Technol.* **2022**, *86*, 834–846. [CrossRef]
21. Zhang, M.; Zhang, K.; Zhou, R.J.; Wang, J.P. Hydroxylamine enhanced activation of peroxymonosulfate by Fe(III)/Cu(II) bimetallic for high-efficiency degradation of AO7. *Water Sci. Tech.* **2022**, *85*, 2038–2050. [CrossRef]
22. Luna, M.D.G.; Sablas, M.M.; Hung, C.M.; Chen, C.W.; Garcia-Segura, S.; Dong, C.D. Modeling and optimization of imidacloprid degradation by catalytic percarbonate oxidation using artificial neural network and Box-Behnken experimental design. *Chemosphere* **2020**, *251*, 126254. [CrossRef] [PubMed]
23. Smaali, A.; Berkani, M.; Merouane, F.; Le, V.T.; Vasseghian, Y.; Rahim, N.; Kouachi, M. Photocatalytic-persulfate- oxidation for diclofenac removal from aqueous solutions: Modeling, optimization and biotoxicity test assessment. *Chemosphere* **2020**, *266*, 129158. [CrossRef] [PubMed]
24. Soleymani, A.R.; Moradi, M. Performance and modeling of UV/Persulfate/Ce (IV) process as a dual oxidant photochemical treatment system: Kinetic study and operating cost estimation. *Chem. Eng. J.* **2018**, *347*, 243–251. [CrossRef]
25. Almuntashiri, A.; Hosseinzadeh, A.; Volpin, F.; Ali, S.M.; Dorji, U.; Shon, H.; Phuntsho, S. Removal of pharmaceuticals from nitrified urine. *Chemosphere* **2021**, *280*, 130870. [CrossRef]
26. Estahbanati, M.; Feilizadeh, M.; Iliuta, M.C. Photocatalytic valorization of glycerol to hydrogen: Optimization of operating parameters by artificial neural network. *Appl. Catal. B-Environ.* **2017**, *209*, 483–492. [CrossRef]
27. Chen, J.Y.; Feng, J.W.; Lu, S.S.; Shen, Z.J.; Du, Y.L.; Peng, L.; Nian, P.; Yuan, S.J.; Zhang, A.Y. Non-thermal plasma and Fe^{2+} activated persulfate ignited degradation of aqueous crystal violet: Degradation mechanism and artificial neural network modeling. *Sep. Purif. Technol.* **2018**, *191*, 75–85. [CrossRef]
28. Mohammadi, F.; Samaei, M.R.; Azhdarpoor, A.; Teiri, H.; Badeenezhad, A.; Rostami, S. Modelling and Optimizing Pyrene Removal from the Soil by Phytoremediation using Response Surface Methodology, Artificial Neural Networks, and Genetic Algorithm. *Chemosphere* **2019**, *237*, 124486. [CrossRef]
29. Yu, M.Z.; Yuan, X.; Li, S.Y.; Hu, J.T.; Li, S.Y.; Zhao, Y.C. Laboratory and simulation study on the adsorption of caffeine onto river sediments and the influencing factors. *Acta Sci. Circumstantiae* **2018**, *38*, 560–569.
30. Cai, Y.; Xing, Y.; Hu, D. On Sensitivity Aaalysis. *J. Beijing Norm. Univ. (Nat. Sci.)* **2008**, *44*, 9–16.
31. Khan, S.U.; Khan, H.; Anwar, S.; Khan, S.; Zanoni, M.V.B.; Hussain, S. Computational and statistical modeling for parameters optimization of electrochemical decontamination of synozol red dye wastewater. *Chemosphere* **2020**, *253*, 126673. [CrossRef] [PubMed]
32. Dong, H.Y.; Fan, S.; Jin, C.J.; Gao, M.C.; She, Z.L.; Zhao, Y.G. Degradation of microcystin-IR by electrochemically activated sulfate: Variable evaluation and model construction using artificial neural network. *Environ. Chem.* **2020**, *39*, 3390–3401.
33. Liu, G.F.; Li, X.C.; Han, B.J.; Chen, L.W.; Zhu, L.N.; Campos, L.C. Efficient degradation of sulfamethoxazole by the Fe(II)/HSO_5-process enhanced by hydroxylamine: Efficiency and mechanism. *J. Hazard. Mater.* **2017**, *322*, 461–468. [CrossRef] [PubMed]
34. Qi, C.D.; Liu, X.T.; Ma, J.; Lin, C.Y.; Li, X.W.; Zhang, H.J. Activation of peroxymonosulfate by base: Implications for the degradation of organic pollutants. *Chemosphere* **2016**, *151*, 280–288. [CrossRef] [PubMed]
35. Rastogi, A.; Al-Abed, S.R.; Dionysiou, D.D. Sulfate radical-based ferrous-peroxymonosulfate oxidative system for PCBs degradation in aqueous and sediment systems. *Appl. Catal. B-Environ.* **2009**, *85*, 171–179. [CrossRef]
36. Ding, Y.M.; Zhang, W.L.; Yu, L.; Lu, K.H. The accuracy and efficiency of GA and PSO optimization schemes on estimating reaction kinetic parameters of biomass pyrolysis. *Energy* **2019**, *176*, 582–588. [CrossRef]
37. Jin, J.L.; Wei, Y.M.; Ding, J. Projection pursuit model for comprehensive evaluation of water quality. *Acta Sci. Circumstantiae* **2001**, *21*, 431–434.